LLNL-TR- 732302

LAWRENCE
LIVERMORE
NATIONAL
LABORATORY

Fast Running Urban Dispersion Model for Radiological Dispersal Device (RDD) Releases: Model Description and Validation

Akshay Gowardhan, Stephanie Neuscamman, John Donetti, Hoyt Walker, Rich Belles, Bill Eme,Steven Homann, Matthew Simpson and John Nasstrom

National Atmospheric Release Advisory Center
Lawrence Livermore National Laboratory
Livermore, CA

May 31, 2017

This work was sponsored by the Department of Homeland Security Science and Technology Directorate's National Urban Security Technology Laboratory (NUSTL)

Disclaimer

This work performed under the auspices of the U.S. Department of Energy by Lawrence Livermore National Laboratory under Contract DE-AC52-07NA27344.

Fast Running Urban Dispersion Model for Radiological Dispersal Device (RDD) Releases: Model Description and Validation

Akshay Gowardhan, Stephanie Neuscamman, John Donetti, Hoyt Walker, Rich Belles, Bill Eme, Steven Homann, Matthew Simpson and John Nasstrom

National Atmospheric Release Advisory Center (NARAC)
Lawrence Livermore National Laboratory

Abstract

Aeolus is an efficient three-dimensional computational fluid dynamics code based on finite volume method developed for predicting transport and dispersion of contaminants in a complex urban area. It solves the time dependent incompressible Navier-Stokes equation on a regular Cartesian staggered grid using a fractional step method. It also solves a scalar transport equation for temperature and using the Boussinesq approximation. The model also includes a Lagrangian dispersion model for predicting the transport and dispersion of atmospheric contaminants. The model can be run in an efficient Reynolds Average Navier-Stokes (RANS) mode with a run time of several minutes, or a more detailed Large Eddy Simulation (LES) mode with run time of hours for a typical simulation.

This report describes the model components, including details on the physics models used in the code, as well as several model validation efforts. Aeolus wind and dispersion predictions are compared to field data from the Joint Urban Field Trials 2003 conducted in Oklahoma City (Allwine et al 2004) including both continuous and instantaneous releases. Newly implemented Aeolus capabilities include a decay chain model and an explosive Radiological Dispersal Device (RDD) source term; these capabilities are described. Aeolus predictions using the buoyant explosive RDD source are validated against two experimental data sets: the Green Field explosive cloud rise experiments conducted in Israel (Sharon et al 2012) and the Full-Scale RDD Field Trials conducted in Canada (Green et al 2016).

1. Introduction and Project Background

The primary objective of this work is to support the development of enhanced atmospheric plume hazard modeling to provide guidance to local emergency response organizations during a radiological incident (such as those involving explosive release of radiological material, or RDD). Within an urban area, the transport and dispersion of airborne contaminants are strongly affected by the size and shape of buildings. Channeling, updrafts, downdrafts, recirculating flows and areas of enhanced or reduced levels of turbulence result in complex plume dispersion patterns and affect the vertical and horizontal spread of contaminants. High-resolution urban models are needed to simulate these key features, which are not currently explicitly resolved in emergency response models. Specifically, a modeling capability integrating radiological source terms, radiological decay processes, and urban flow and dispersal is essential for first responders, emergency managers and other response personnel in the initial hours of a response to a radiological or nuclear incident. Improved models that resolve individual buildings effects will increase the capability to protect citizens and responders from radiological hazards during an emergency.

The Department of Energy's Lawrence Livermore National Laboratory (LLNL) National Atmospheric Release Advisory Center (NARAC) has developed a fast-running Computational Fluid Dynamics (CFD) model, Aeolus

(Lucas et al., 2016), that can accurately model the dispersion of airborne contaminants in urban settings, for distances up to 10 km downwind of the incident. This report details the ongoing development of enhanced modeling capabilities for the existing Aeolus model, sponsored by DHS NUSTL, to create a tool to conduct rapid radiological contaminant modeling and analysis and produce urban model predictions for use by emergency responders. The work leverages previous and existing DOE/NARAC, DHS, and FEMA efforts to develop radiological/nuclear response tools and user products, and is being done in a manner that is coordinated with the Interagency Modeling and Atmospheric Assessment Center (IMAAC).

This report provides details on the Aeolus wind and dispersion models and their validation using field data for both continuous and instantaneous release of a tracer gas from Joint Urban 2003 experiment. The model improvements conducted in the first two years of the current DHS NUSTL project are also described. During the first year of this project, we have added radiological decay and particle deposition to the Aeolus model. A suitable deposition model has been incorporated to predict the deposition of radiological materials on the ground and building surfaces, including gravitational settling of larger particles modeled using the concept of a settling velocity. Radiological decay using the Bateman equations has also been implemented in Aeolus. The newly implemented Aeolus capabilities are compared to additional experimental datasets and the model performance is evaluated. During the second year of this project, we validated Aeolus model performance for instantaneous releases in an urban environment and implemented a dynamic cloud rise model – the Sandia National Laboratories' -developed PUFF model – to predict the initial behavior of an explosive (RDD) release in Aeolus. Aeolus model results for an instantaneous release are compared to data from the using field data from Joint Urban 2003 experiment. The explosive source implementation is validated against the Israel Greenfield experiments (Sharon et al. 2012) and the and the Full-Scale Canadian RDD trials (Green et al. 2016). Finally, a discussion of project goals and tasks for the final year of the project is included in Section 6.

2. Aeolus Model Description

This section provides details on the components of the Aeolus model. Section 2.1 describes the two modes for solving the 3D wind flow field: RANS and LES. Section 2.2 describes the Aeolus dispersion model.

2.1 Aeolus Wind Model

RANS. Aeolus can be run efficiently using a RANS model. The model produces a steady state solution for the 3D wind velocity field. The wind is based on the 3D RANS equations for incompressible flow using a zero equation (algebraic) turbulence model based on Prandtl's mixing length theory (Gowardhan et al., 2011). The selection of zero-equation turbulence model was made in order to reduce the run time of the CFD simulation, making it more applicable for use in fast-response applications (Chen and Xu, 1998). It is accepted, however, that more complex turbulence models could also be considered, however, given that there has been no evidence of clear superiority or appropriateness of one model over another for all wind flow applications in complex urban geometries, using a zero-equation model was considered acceptable in the context of this exercise.

The governing RANS equations are solved explicitly in time until steady state is reached using a projection method. At each time step of the projection method, the divergence-free condition is not strictly satisfied to machine precision levels, but rather when steady state is reached incompressibility is recovered. This makes the method comparable to the artificial compressibility method (Chorin, 1967). The RANS equations are solved on a staggered mesh using a finite volume discretization scheme that is second-order accurate in space (central difference) and time (Adams–Bashforth). The law-of-the-wall is imposed on all the solid surfaces. The pressure Poisson equation is solved using the successive over-relaxation method (SOR). A free slip condition is imposed at the top boundary and the side boundaries, while an outflow boundary condition is used at the outlet.

LES. Aeolus can be run in a high-fidelity mode using the Large eddy simulation (LES) model. LES resolves the large scales of the flow field solution, allowing better fidelity than alternative approaches such as Reynolds-averaged Navier–Stokes (RANS) methods. It also uses a turbulence closure model to account for the sub-grid scales of the flow field, rather than resolving them as direct numerical simulation (DNS) does. This makes the computational cost for practical engineering systems with complex geometry or flow configurations attainable using multiple processors. In contrast, direct numerical simulation, which resolves every scale of the solution, is prohibitively expensive for nearly all systems with complex geometry or flow configurations.

Numeric Methods. The model uses a second order accurate central difference and QUICK scheme (Leonard 1979) to solve for the advective terms and a second order accurate central difference scheme for diffusive terms. The temporal integration is performed using the Adams-Bashforth scheme (Bashforth and Adams 1883), which is also second order accurate. The pressure Poisson equation is solved efficiently using a multigrid technique (Brandt and Livne, 2011).

Turbulence closure. For the RANS model, we have opted for one of the simplest approaches to the closure problem, namely, the zero-equation model (Baldwin and Lomax, 1978, Smith and Cebeci, 1967). Based on the assumption that there exists an analogy between the action of viscous stresses and Reynolds stresses on the mean flow, a simplified zero equation (algebraic) turbulence model based on Prandtl's mixing length theory is used (Prandtl, 1925)

$$\upsilon_T = (l_{mix})^2 \sqrt{\overline{S_{ij}}\,\overline{S_{ij}}}$$

The mixing length $l_{mix} = ky$, where y is the shortest distance to any building wall or the ground and k is the von-Karman constant and $\overline{S_{ij}} = \frac{1}{2}\left(\frac{\partial \overline{u_i}}{\partial x_j} + \frac{\partial \overline{u_j}}{\partial x_i}\right)$.

When Aeolus is used in LES mode, a simple Smagorinsky model (Smagorinsky, 1963) is used:

$$\upsilon_T = (c_s \Delta)^2 \sqrt{\overline{S_{ij}}\,\overline{S_{ij}}}\,.$$

where $\Delta = \sqrt[3]{dxdydz}$ and $\overline{S_{ij}} = \frac{1}{2}\left(\frac{\partial \overline{u_i}}{\partial x_j} + \frac{\partial \overline{u_j}}{\partial x_i}\right)$.

2.2 Aeolus dispersion model

To model dispersion within the atmosphere, Aeolus solves the three-dimensional, incompressible, advection-diffusion equation with sources and sinks:

$$\frac{\partial \bar{c}}{\partial t} + \bar{u}\frac{\partial \bar{c}}{\partial x} + \bar{v}\frac{\partial \bar{c}}{\partial y} + \bar{w}\frac{\partial \bar{c}}{\partial z} = \frac{\partial}{\partial x}\left(\nu_t \frac{\partial \bar{c}}{\partial x}\right) + \frac{\partial}{\partial y}\left(\nu_t \frac{\partial \bar{c}}{\partial y}\right) + \frac{\partial}{\partial z}\left(\nu_t \frac{\partial \bar{c}}{\partial z}\right) + Q$$

where $\bar{c}$ is the mean air concentration of the species; $\bar{u}$, $\bar{v}$, and $\bar{w}$ are the mean wind components in the x, y, and z projection directions respectively; ν_t is the eddy diffusivity and Q is the source term.

Aeolus solves the stochastic differential equations that describe the same process as above within a Lagrangian framework (Durbin, 1983). The equations for the particle displacement due to advection, diffusion, and settling in the three coordinate directions are:

$$dx = \bar{u}dt + \frac{\partial \nu_t}{\partial x}dt + (2\nu_t)^{1/2} dW_x$$
$$dy = \bar{v}dt + \frac{\partial \nu_t}{\partial y}dt + (2\nu_t)^{1/2} dW_y$$
$$dz = \bar{w}dt + \frac{\partial \nu_t}{\partial z}dt + (2\nu_t)^{1/2} dW_z$$

where $dW_{x,y,z}$ are three independent random variates with zero mean and variance dt. The stochastic differential equations above are then integrated in time to calculate an independent trajectory for each particle. The ensemble-mean concentration, at any time t, can then be calculated from the particle locations at time t and the contaminant mass associated with each particle.

3. Aeolus model validation

Aeolus was validated using data from the Joint Urban 2003 field experiment, which was performed in July 2003 in the central business district of Oklahoma City. A large number of meteorological instruments and tracer-gas air samplers where deployed in the urban area: meteorological measurements were taken at over 160 different locations (Allwine et al., 2004) while tracer measurements were made at over 130 locations (Clawson et al., 2005). Ten intensive operation periods (IOPs) were conducted for both daytime periods and for nighttime periods in which most all meteorological and tracer sampler instrumentation were activated. During the IOPs, the winds were predominantly from the south. Further details about the experiment, instrument types and locations, and tracer release information can be found in Allwine et al. (2004), Clawson et al. (2005), Flaherty et al. (2007), Nelson et al. (2007) and Brown et al. (2004).

3.1 Continuous release

Aeolus results were compared to 12 trials (daytime and nighttime) with continuous releases. The winds were predominantly from the south. The portable wind detector at the Post Office (PWID 15), a propeller anemometer, was used to record the 'wake-free' inflow profile for wind direction and wind speed. It was located ~500 m upstream of the central business district (CBD) area at 50 m above ground on a 35 m rooftop tower, and was free from building effects. SF_6 gas was released continuously for 30 minutes from different locations shown in Figure 1 and listed in Table 1.

The computational domain used was 1.4 km x 1.4 km x 0.2 km discretized on a regular grid ($dx = dy = 5$ m, $dz = 3$ m, Figure 2). The horizontal grid spacing was chosen as 5 m as it is the minimum grid spacing needed to resolve a typical street canyon. The grid consists of ~ 4.5 million control volumes (Table 2). The Aeolus RANS wind simulation took less than 300 seconds while the dispersion simulation took around 80 seconds. Simulations were performed on 2011 MacBook pro running Mac OS X version 10.6.8 on a 2Ghz Intel Core i7 processor (4 cores) with 8 Gb 1333 MHz DDR3 memory. The Lagrangian dispersion model uses only single processor while the wind model uses all the available 4 processors.

Table 1: Description of test cases for continuous releases from Joint Urban 2003 experiments used in Aeolus model validation.

	IOP#	Julian Date & UTC Time	Wind Rose Plot (PWID 15), ~500 m	Mean Wind	Mean Wind	Amount Released	Release Location

			South of Release Location (@50 m AGL)	Speed (m/s)	Direction (degrees)	(g) (30 min Continuous Release)	
a)	IOP 2 Trial 3	2003183, 1800-1830 UTC (Daytime Release)	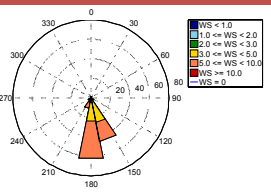	5.20	171.0	8891	Westin Hotel
b)	IOP 3 Trial 1	2003188, 1600-1630 UTC (Daytime Release)	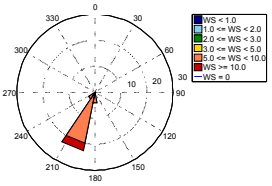	7.44	202.8	8890	Botanical Garden
c)	IOP 3 Trial 2	2003188, 1800-1830 UTC (Daytime Release)	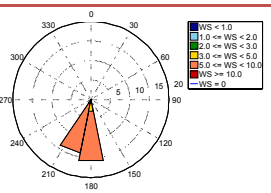	6.50	190.5	5443	Botanical Garden
d)	IOP 3 Trial 3	2003188, 2000-2030 UTC (Daytime Release)	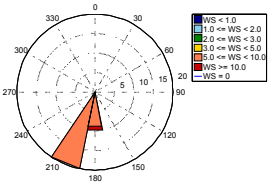	7.60	194.5	5443	Botanical Garden
e)	IOP 8 Trial 1	2003206, 0400-0430 UTC (Nighttime Release)	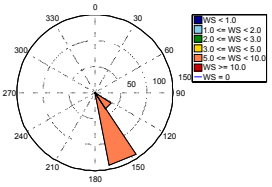	6.82	153.1	5534	Westin Hotel
f)	IOP 8 Trial 2	2003206, 0600-0630 UTC (Nighttime Release)	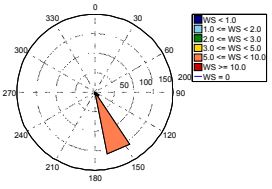	6.80	157.0	5488	Westin Hotel
g)	IOP 8 Trial 3	2003206, 0800-0830 UTC (Nighttime Release)	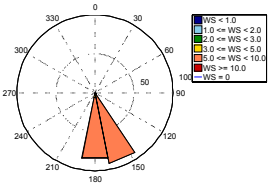	7.15	168.2	5352	Westin Hotel
h)	IOP 9 Trial 1	2003208, 0400-0430 UTC (Nighttime Release)	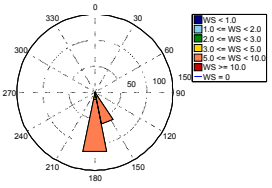	6.12	172.0	3583	Park Avenue

i)	IOP 9 Trial 2	2003208, 0600-0630 UTC (Nighttime Release)	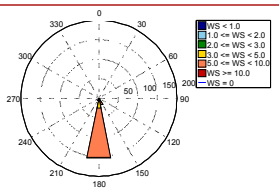	6.30	178.0	5488	Park Avenue
j)	IOP 9 Trial 3	2003208, 0800-0830 UTC (Nighttime Release)	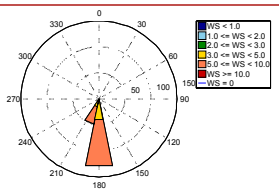	5.75	187.1	3765	Park Avenue
k)	IOP 10 Trial 1	2003210, 0600-0630 UTC (Nighttime Release)	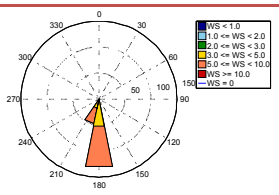	5.30	188.2	4037	Park Avenue
l)	IOP 10 Trial 2	2003210, 0800-0830 UTC (Nighttime Release)	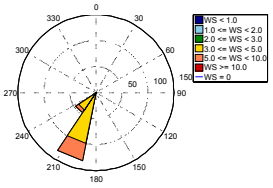	4.44	210.2	3493	Park Avenue

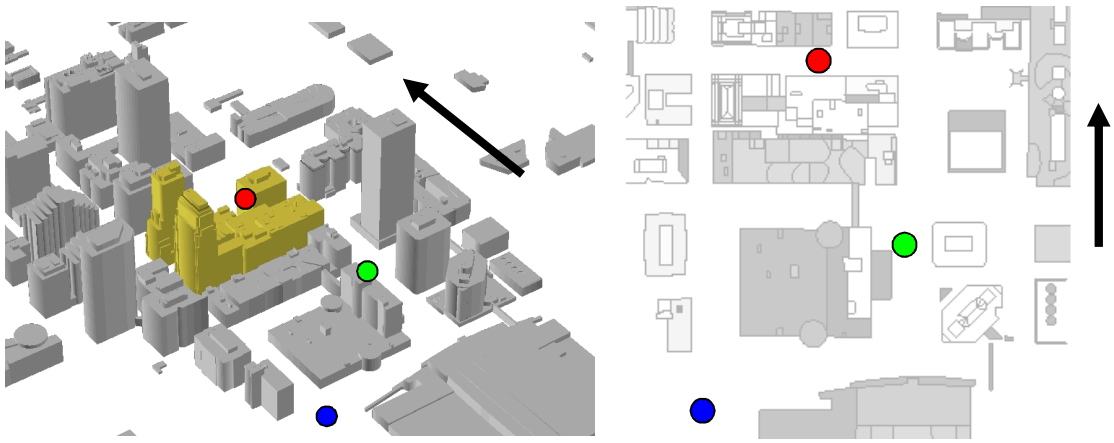

Figure 1: SF_6 release locations in the Oklahoma City CBD during JU 2003 (● Park Avenue, ● Westin and ● Botanical).

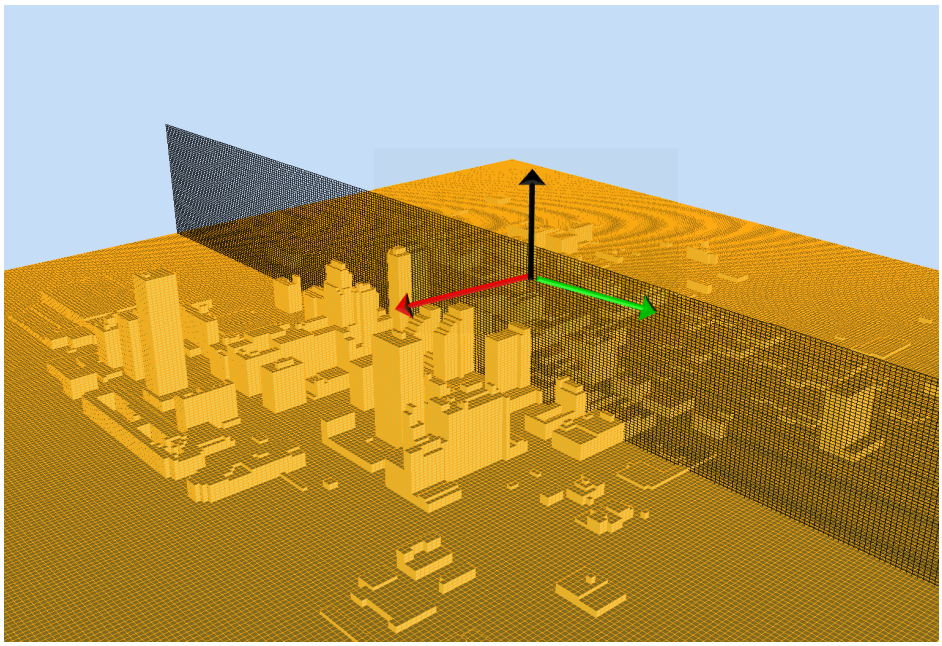

Figure 2: Aeolus computational domain showing gridded buildings of the CBD. A slice shows the grid spacing in the vertical direction.

Table 2: Simulation parameters for Aeolus wind and Lagrangian dispersion models used in the Joint urban 2003 model validation study.

Simulation Parameters	
Wind Model	**Plume Model**
Resolution: dx = 5m, dy = 5m, dz = 3m, uniform grid	Resolution: dx = 5m, dy = 5m, dz = 3m, uniform grid
Domain: L_x = 1350m, L_y = 1350m, L_z = 180m	Domain: L_x = 1350m, L_y = 1350m, L_z = 180m
Grid Points: nx = 271, ny = 271, nz = 61, ~ 4.5 Million	Grid Points: nx = 271, ny = 271, nz = 61, ~ 4.5 Million
Roughness length for inflow profile, z_o= 0.5m	Number of particles released = 1,000,000
30 min averaged winds speed and wind direction from PWID 15 (@ 50 m AGL) were used to construct a logarithmic inflow profile (z_o= 0.05 m)	Simulation duration = 3600 sec
	Averaging interval = 1800 sec

Aeolus RANS model results. Figure 3 shows velocity vector plots for flow around Oklahoma City in the x-z plane at 8 m above ground level (AGL). Simulated wind vectors from the Aeolus model (grey arrows) are overlaid with meteorological observations (black arrows). Longer arrows in Figure 3 indicate higher wind speed. The Aeolus wind speed prediction is also represented by the color shading around the buildings, where warmer colors indicate higher predicted wind speed values. From this figure, it can be observed that the Aeolus model is able to predict the important flow features reasonably well. The model captures the channeling effects along north-south running streets and is able to predict the high velocity measured in these regions. The model also well predicts the reverse flow in the street canyons and wake regions in the domain. The model produced velocity in the intersection areas are in good agreement with the field data.

Figure 4 shows the measured and predicted air concentration values at ground level for the selected Joint Urban field trials. The colored circles represent the experimentally measured air concentration value averaged over the 30 minutes of the continuous release. The colored contours represent the Aeolus prediction of the 30 minute average air concentration, with higher predicted concentration values near the source (red, orange areas). The Aeolus model generally predicts the experimental results well; the areas of highest concentration and the general amount of down-wind spreading are captured in the simulation results.

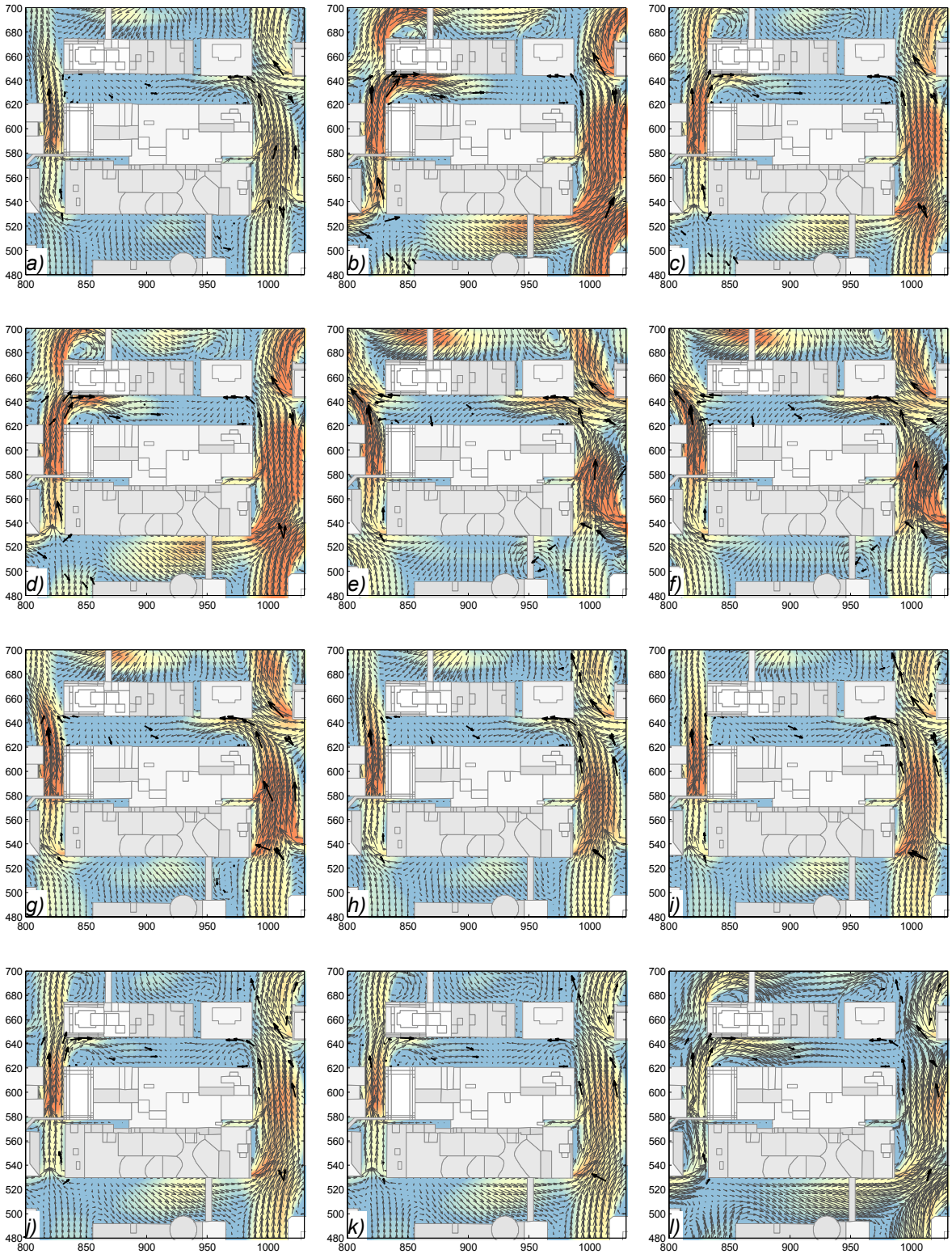

Figure 3: Velocity vectors from the simulation results (gray arrow) overlaid with 30 min averaged field data (black arrows) for selected trials during Joint urban 2003 field experiment: horizontal slice (*xy* plane) at 8m AGL.

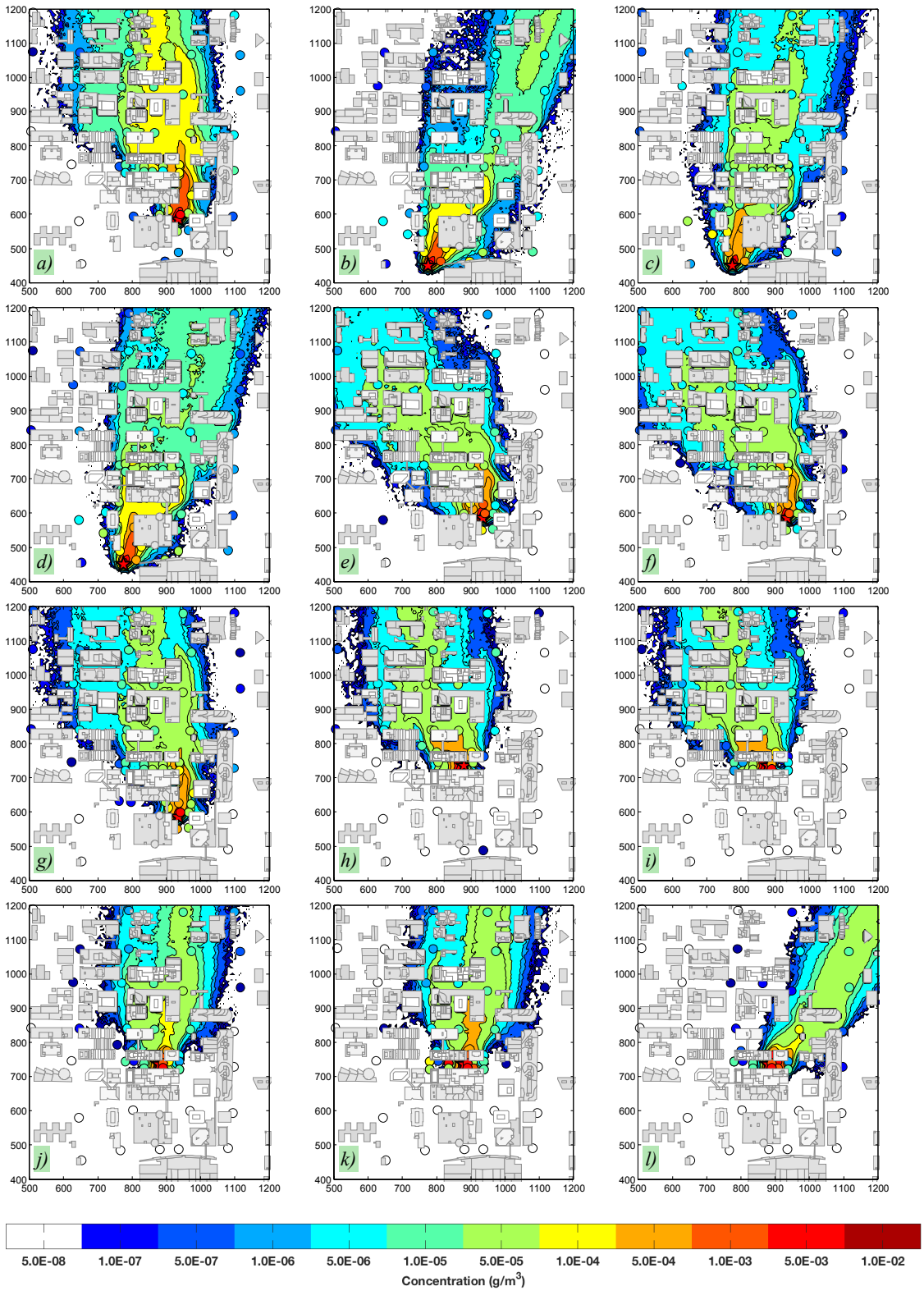

Figure 4: Contours of 30-minute averaged air concentration (g/m^3) from Aeolus overlaid with 30 min averaged field concentration data (filled circle) for selected trials during Joint Urban 2003 field experiment: horizontal slice (xy plane) at 2 m AGL.

Table 3: Quantitative analysis of Aeolus simulation results compared to Joint urban 2003 experimental data

	IOP#	FAC 2 (%)	FAC 5 (%)	FAC 10 (%)	|FB|	NMSE	Wind Model runtime (sec)	Plume Model runtime (sec)	Total runtime (sec)
a)	IOP2, Tr3	20.5	65.3	75.64	0.3118	0.6538	203.70	82.70	286.40
b)	IOP3, Tr1	25.6	52.5	62.82	0.3706	2.121	202.70	67.10	269.80
c)	IOP3, Tr2	26.5	59.0	67.47	0.0310	1.2046	207.72	85.88	293.60
d)	IOP3, Tr3	42.1	62.6	72.28	0.0703	0.3311	203.53	78.93	282.46
e)	IOP8, Tr1	39.7	84.3	90.36	0.5817	16.508	204.12	83.76	287.88
f)	IOP8, Tr2	30.1	79.5	89.15	0.8394	17.014	211.17	82.14	293.13
g)	IOP8, Tr3	32.5	75.9	85.54	0.1614	0.5701	202.25	74.93	277.18
h)	IOP9, Tr1	26.5	85.5	91.56	0.3117	3.758	204.23	83.54	287.77
i)	IOP9, Tr2	22.8	78.3	85.54	0.1453	2.3184	201.55	79.21	280.76
j)	IOP9, Tr3	25.3	90.3	97.59	0.0284	0.9707	198.62	72.33	270.95
k)	IOP10, Tr1	20.4	78.3	85.54	0.1782	2.6237	199.64	78.09	277.73
l)	IOP10, Tr2	18.0	72.2	78.31	0.2981	1.8097	208.27	84.62	292.89
	Average	27.5	73.6	81.82	0.2773	4.1569	**203.95**	**79.43**	**283.38**

The Aeolus model predictions of the average air concentration can also be evaluated using standard atmospheric modeling comparison metrics to quantitatively measure model performance. Table 3 shows several metrics comparing the Aeolus predictions to measured data for each of the considered releases. The final row of Table 3 gives the average value for each metric from the 12 simulations.

The FAC numbers presented are the fraction of values where the ratio between the observed measurement (M) and predicted (C) values - or the predicted and observed values for symmetry – are less than a certain number. For example, FAC 5 would capture the proportion of values where M/C or C/M are less than 5; FAC5: $1/5 < (M/C) < 5$. The FAC is a standard plume model evaluation statistic, and can be used to assess overall absolute model errors. Higher FAC values indicate better agreement between simulation and measurements. In previous studies, Foster et al (2000) found that for NARAC's LODI model, very stringent point-to-point comparisons of this type were typically within a factor of 2 of the measured data (FAC2 >50%) for simpler terrain, meteorological and source conditions. For complicated scenarios, such as those involving complex terrain or obstacles, energetic releases, or rapidly varying meteorology, FAC10>50% is considered reasonable agreement between measured and predicted values. Dispersal in an urban environment would represent a complicated case, so the values shown in Table 3 show good agreement between modeled and measured values, with FAC5>50% for all cases considered.

Table 3 gives further quantitative analysis of results in terms of absolute value of fractional bias (|FB|) and the normalized mean square error (NMSE) for concentration. Fractional bias is a normalized value of mean error (Warner et al 2006). |FB| values range from 0 to +2. A perfect agreement between model and measurement would result in FB=0.

$$FB = \overline{\left(\frac{(C_i - M_i)}{0.5(C_i + M_i)}\right)}$$

where M_i is the i^{th} observation (measurement), and C_i is the corresponding model prediction. NMSE captures the overall absolute departure of the modeled results from measurements. Lower values of NMSE indicate better agreement between model and experimental values.

$$NMSE = \frac{\frac{1}{N}\sum(C_i - M_i)^2}{\bar{M}^2}$$

where M_i and C_i are as above, N is the number of valid measurement-model data pairs, and $\bar{M}$ is the mean measurement value. Hanna and Chang (2012) suggest following limits on the comparison metrics for acceptable performance an urban model:

- |FB| ≤0.67, i.e., the relative mean bias less than a factor of ~2
- NMSE ≤6, i.e., the random scatter ≤2.4 times the mean
- FAC2 ≥0.30, i.e., 30% or more of model predicted values are within a factor of two of measured values

The Aeolus comparison results shown in Table 3 fulfill each of these limits, on average, indicating that the model is performing well.

Table 3 also shows the simulation run time for both the wind and dispersion models for each of the cases and the average values over all the simulations using the computer hardware described previously. The Aeolus wind and dispersion models can both be run in less than five minutes total run time. Using Aeolus, accurate predictions of dispersion of material in an urban area can be rapidly generated and provided to decision makers in the case of a hazardous atmospheric release.

Figure 5 displays scatter plots of the paired (point-to-point) values from the Aeolus predictions and the field experiment observed measurements. Data points (blue circles) that fall on the solid black diagonal represent perfect matching between the predicted and measured values. Points above the black line represent values that were over-predicted by the Aeolus simulation and points below the line are under-predicted by Aeolus compared to the measured data. The colored diagonal lines represent FAC2, FAC5, and FAC10 values, with increasing FAC number away from the center (black) line. The scatter plots also show good agreement between predicted and measured values, with most pairs falling within the FAC5 lines. Figure 5 also indicates the number of matched zeros, which show how often the model correctly predicts zero valued measurements (data where the measurement was below the instruments minimum level of detection, MLOD). A finite number of matched zero values represent that the model is able to correctly predict the spread of the plume.

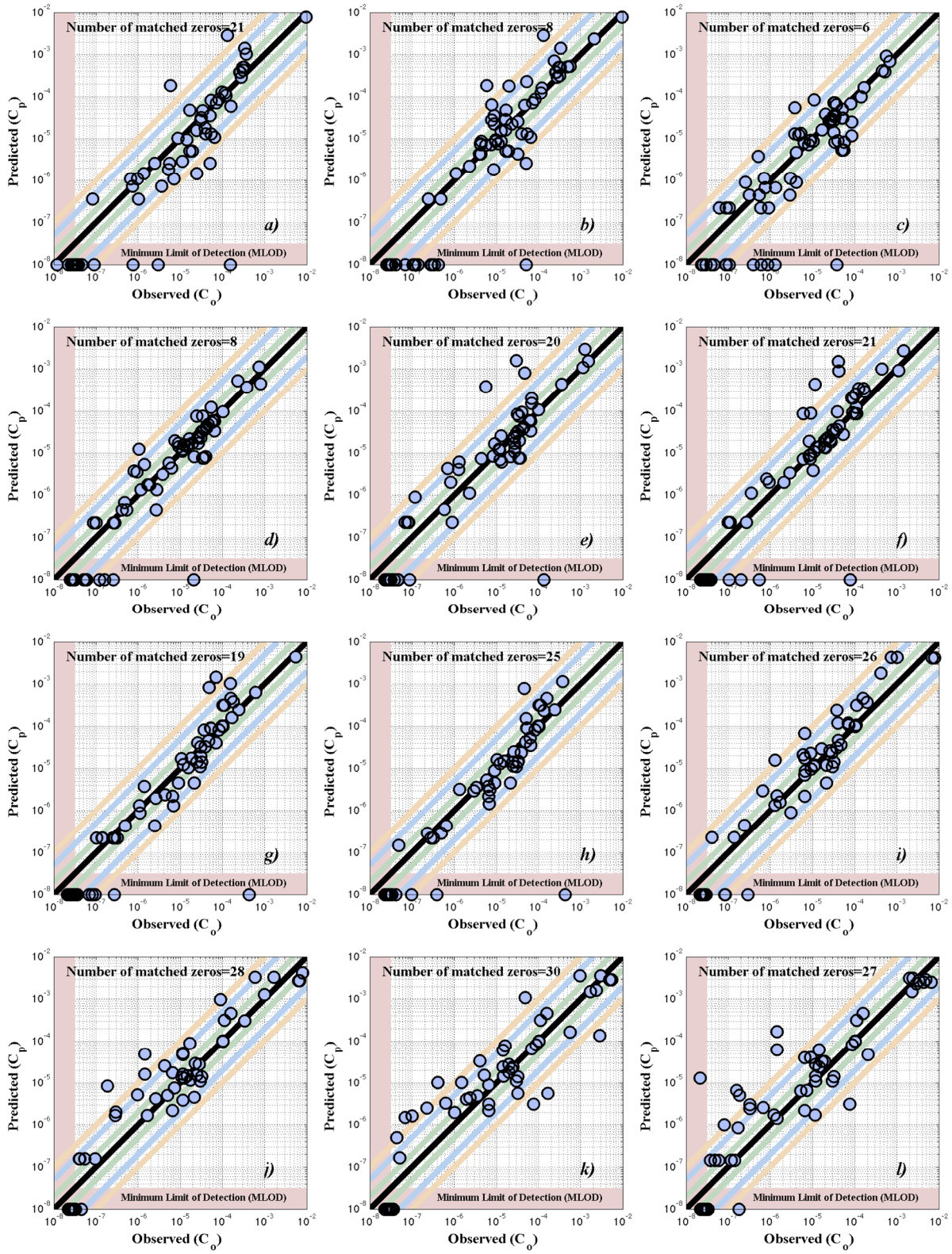

Figure 5: Paired in time and space scatter plot for predicted and observed 30 min averaged concentration (g/m3) for *selected trials* during Joint urban 2003 field experiment: horizontal slice (*xy* plane) at 2 m AGL.

Aeolus LES model results. Aeolus simulation of one event, IOP 8 trial 2 (see case f, Table 1), was conducted using LES mode. The event was chosen because the winds were consistently from the south with little variation and the edge of the plume was well captured in the measured data (SF_6 gas samplers). Time varying input for the simulation was constructed using data from the PWID 15 anemometer. Six log–law profiles (5 min average) were used in the LES simulation. Figure 6 shows the wind speed and direction measured by the anemometer (dashed lines) and the five minute averaged values used to construct the Aeolus input wind profile (solid line, squares). The averaged log-law profiles were superimposed with random perturbation with a standard deviation of 10% of the wind speed and a zero mean to perturb the inflow and thus creating a turbulent inflow profile.

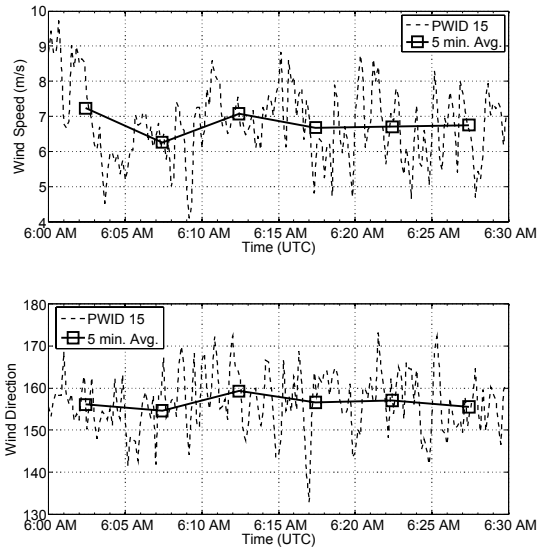

Figure 6: Meteorological input to the Aeolus LES simulation was 5 min. average data from PWID15 with random perturbations superimposed of the inflow profile.

Figure 7 shows air concentration results at ground level measured during IOP 8 (test case f) and predicted by the Aeolus LES and Aeolus Lagrangian dispersion models. The colored circles represent the experimentally measured air concentration value averaged over the 30 minutes of the continuous release. The colored contours represent the Aeolus prediction of the 30-minute average air concentration, with higher predicted concentration values near the source (red, orange areas). Comparing Figure 7 to Figure 4(f), the LES mode predicts greater plume spreading in the cross-wind direction, captures some additional channeling effects, and predicts more upwind dispersion of the material very close to the release location than the RANS mode results. Figure 8 shows the scatter plots of the paired (point-to-point) values from the Aeolus LES simulation and the values measured in the field experiment.

Compared to the model comparison metrics discussed for the RANS simulations, the LES simulation results are similar or improved using the LES mode in Aeolus for this test case. Using LES, each of the FAC values increased (improved) over the RANS values. For LES: FAC2 = 38.9%; FAC5 = 84.7%; FAC10 = 91.5%. The fractional bias was similar (0.94 for LES, 0.84 for RANS). The NMSE was much less for the LES simulation (1.381 vs 17.014 for RANS), indicating lower error when comparing to the experimental data. Using the time-varying, high-fidelity model gives better agreement to experimentally measured air concentration values. However, the simulation run time must also be considered. For the LES model, the total run time was ~160 minutes. The RANS model required less than five minutes to produce the results. This exercise confirms that Aeolus LES can possibly be used to make more accurate urban dispersion predictions, but the time required to arrive at the result is much longer than a similar prediction from the RANS model.

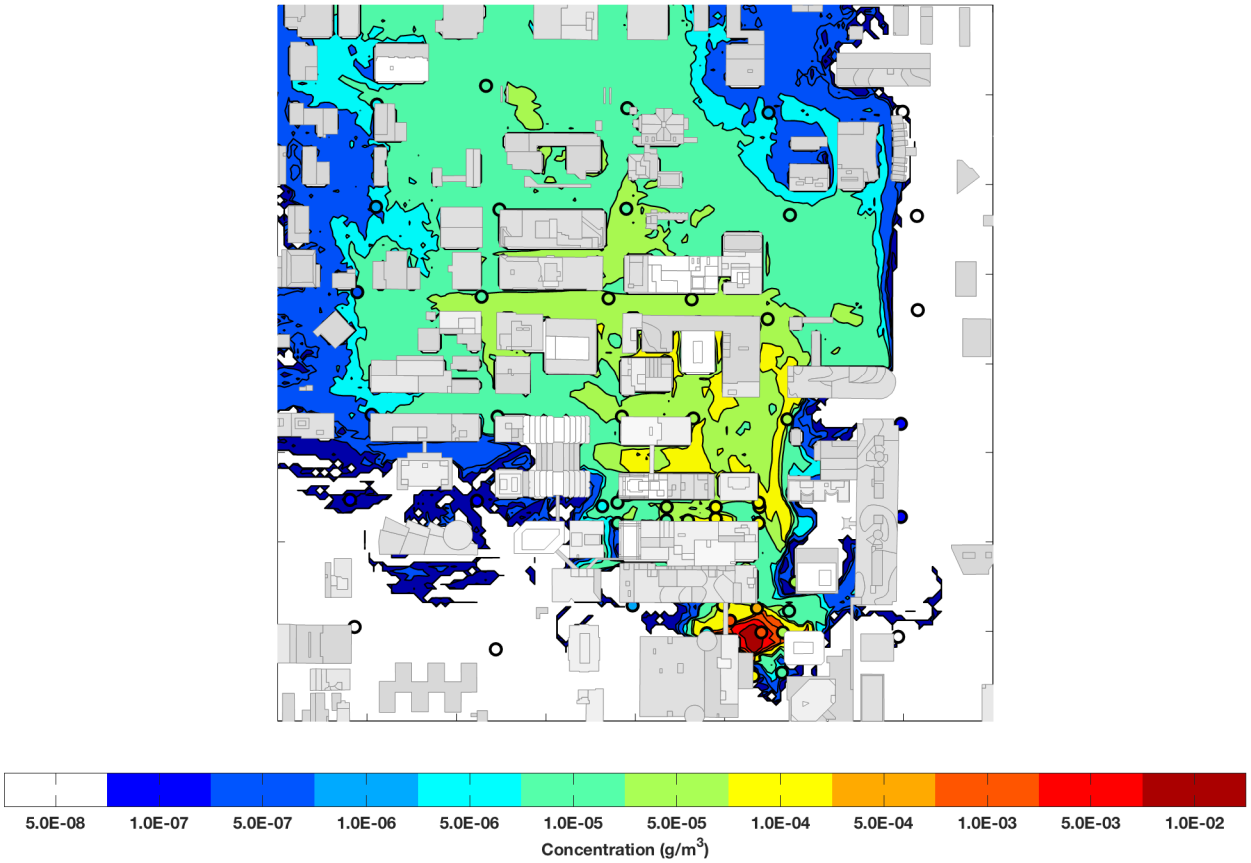

Figure 7: Contours of 30-minute averaged air concentration (g/m^3) from Aeolus LES overlaid with 30 min averaged field concentration data (filled circle) for IOP 8 (test case f) during Joint Urban 2003 field experiment: horizontal slice (xy plane) at 2 m AGL.

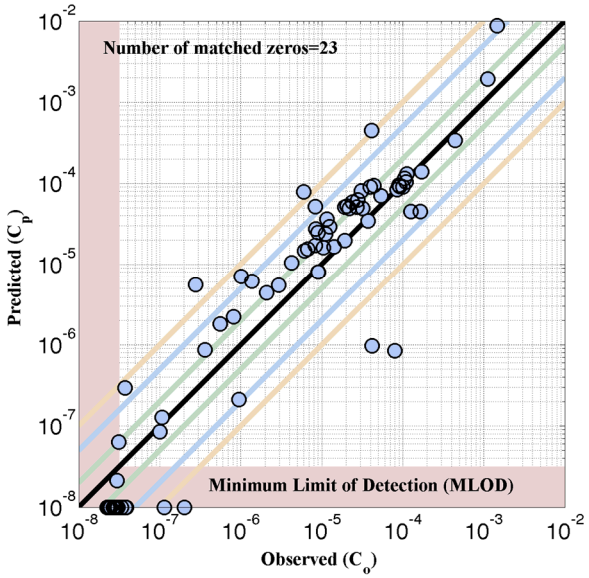

Figure 8: Paired in time and space scatter plot for predicted and observed 30 min averaged concentration (g/m^3) for LES simulation of case (f).

3.2 Instantaneous release

To compare Aeolus RANS predictions with an instantaneous release, we focused on 4 trials during IOP 8. The winds were predominantly from the south. The portable wind detector at the Post Office (PWID 15), a propeller anemometer was used for determining the inflow profile for wind direction and wind speed. It was located ~500 m upstream of the central business district (CBD) area at 50 m above ground on a 35 m rooftop tower free from building effects. SF_6 gas was released instantaneously at four occasions (20 min. apart) from the Westin location shown in Figure 1 and monitored for 20 minutes, as listed in Table 5.

The domain used was 1.4 km x 1.4 km x 0.2 km discretized on a regular grid ($dx = dy = 5$ m, $dz = 3$ m, Figure 2). The grid consists of ~ 4.5 million control volumes (Table 2). The Aeolus RANS wind simulation completed in less than 300 seconds while the Lagrangian dispersion simulation required around 30 seconds.

Table 5: Description of validation test cases for instantaneous release.

	IOP#	Julian Date & UTC Time	Wind Rose Plot (PWID 15), ~500 m South of Release Location (@50 m AGL)	Mean Wind Speed (m/s)	Mean Wind Direction (degrees)	Amount Released (g) (Instan-taneous Release)	Release Location
a)	IOP 8 PUFF #1	2003183, 1000 UTC (Daytime Release)	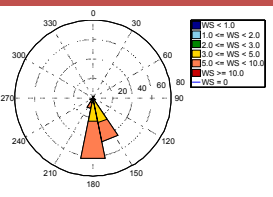	5.20	171.0	500	Westin Hotel
b)	IOP 8 PUFF #2	2003183, 1020 UTC (Daytime Release)	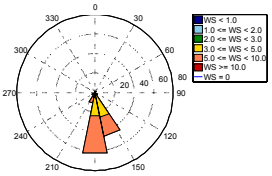	5.20	171.0	500	Westin Hotel
c)	IOP 8 PUFF #3	2003183, 1040 UTC (Daytime Release)	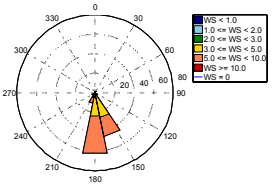	5.20	171.0	300	Westin Hotel
d)	IOP 8 PUFF #4	2003183, 1100 UTC (Daytime Release)	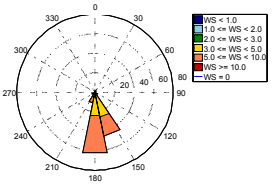	5.20	171.0	305	Westin Hotel

Figure 9 compares the ground level (2 m AGL) predicted concentration with the observed data at different locations inside the CBD. The initial concentrations predicted by Aeolus are higher than observed values (Time = 1 min, upper left), however, by Time = 3 min (upper center), the agreement between the measured values and the Aeolus contours is generally good. Channeling effects evident in measured air concentration are also captured in the Aeolus simulation (see, for example, green contour level in Time = 5 min, upper right). The plume passage time is predicted well by the model, showing most the material has moved beyond the measurement locations by Time = 15 min past the material release time.

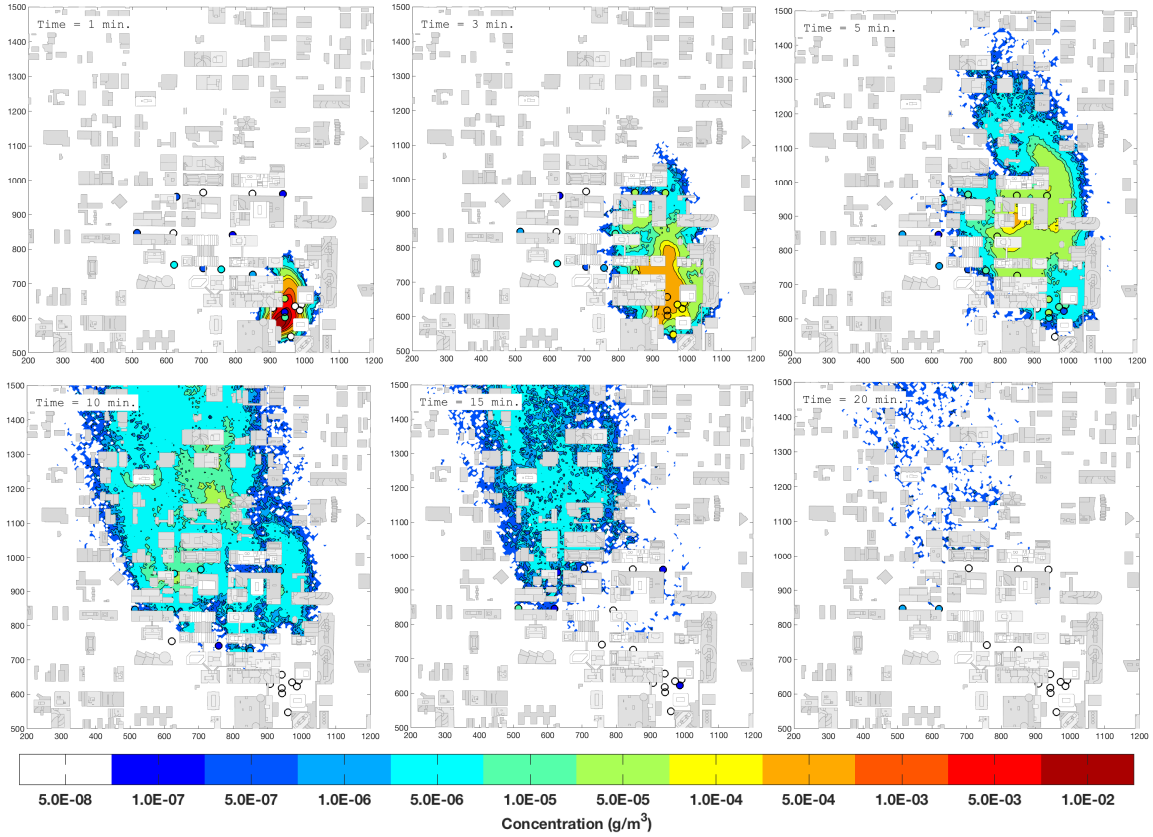

Figure 9: Contours of 1 minute averaged air concentration (g/m^3) from Aeolus overlaid with 1 min averaged field concentration data (filled circle) for the first puff trial of IOP 8 during Joint Urban 2003 field experiment: horizontal slice (xy plane) at 2 m AGL.

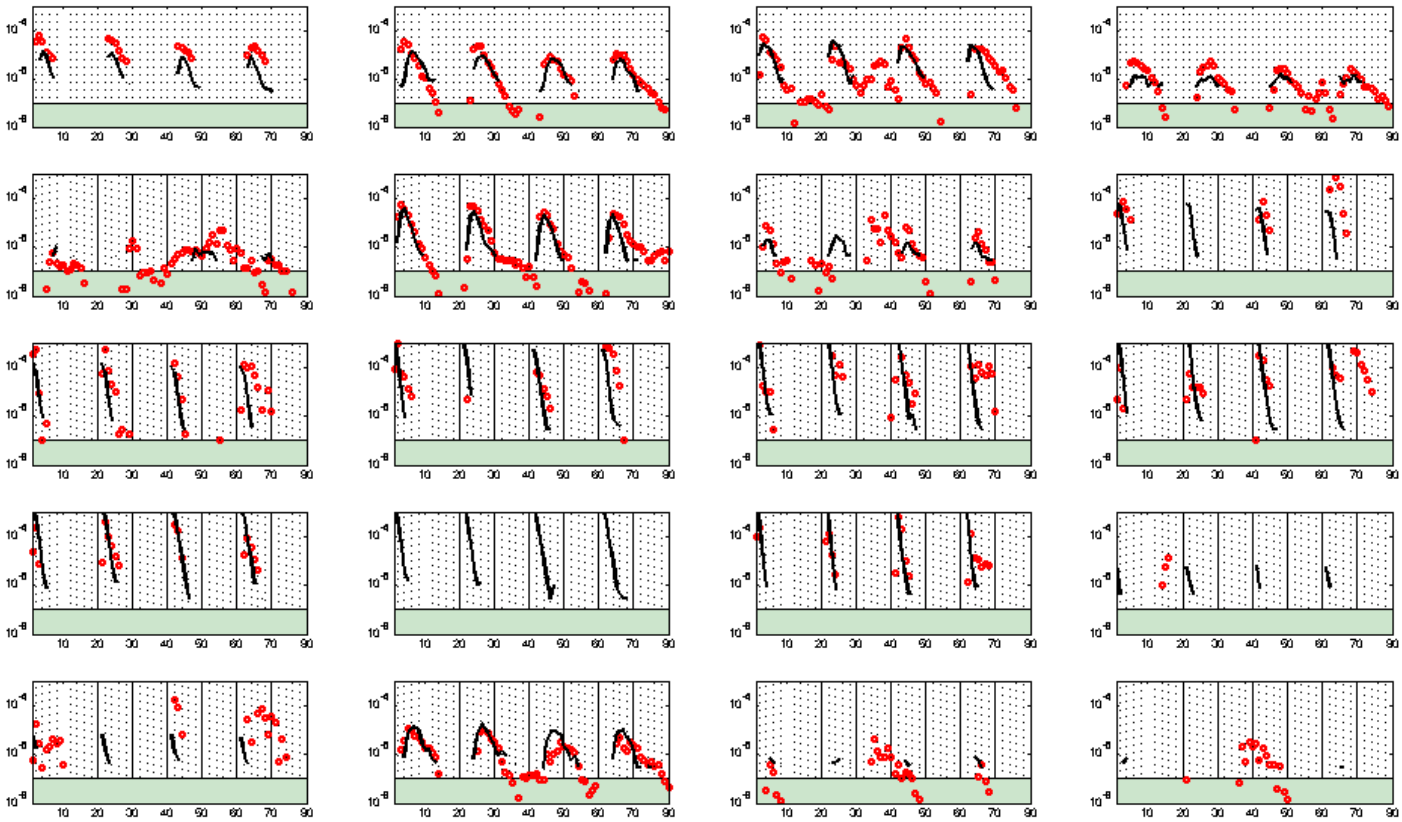

Figure 10: Time series (min) of predicted and observed 1 min averaged air concentration (g/m^3) at 2 m AGL for the 4 instantaneous releases during IOP8 of Joint Urban 2003 field experiment. Each sub-figure shows the predicted (–) and measured (o) values of air concentration values at different sampler locations within the CBD.

Figure 10 shows the measured and predicted values of air concentration (1 minute averages) for the entire IOP8 timeframe. Each sub-figure represents the air concentration results measured (or predicted) at a sensor location (total 20 sensors). The black lines are the Aeolus predicted air concentration and the red circles represent the measured values over the 90 minute time frame. Four puffs were released over the course of the IOP, and Aeolus predicts four noticeable increases (and subsequent decreases) in concentration corresponding to the arrival of the puff releases at most sensor locations. The measured data also shows four distinct concentration peaks corresponding to the puff passage over the sensor in many of the cases in Figure 10. Generally, agreement between the simulation and experiment is good. Some sensor locations show excellent agreement between the data sets, with Aeolus predicting the rise time, peak concentration, and tapering off of air concentration well. At one sampler location, Aeolus predicts material where none was measured, however, this may be the result of local flow phenomena (such as traffic or vegetation) which are not included in the model.

4. Aeolus Model Enhancements (FY16-17)

4.1 Deposition Model

A RDD release in an urban area will lead to deposition of radioactive substance on the building walls and will lead to many aspects associated with an urban RDD clean-up that have never been faced in legacy site remediation, including demolition and destructive technologies, business interests, etc. One of the most important aspect is reducing the time required to decontaminate and return a city to normal use as it can have a tremendous economic and political impact.

Due to above reasons, it is important to understand the deposition process in urban areas and model it correctly. The larger particles will tend to deposit near the source while the smaller particles will travel further downwind. Further, the particles will deposit on the building walls (vertical) as well as on the ground. These phenomena will lead to a complicated deposition pattern in the urban area.

The above-mentioned phenomenon of deposition of gases and aerosols is computed internally in the Aeolus Lagrangian dispersion model using a method similar to LODI's implementation of deposition model. When the particles are within one grid cell of any surface (vertical or horizontal) a fraction of the particle mass (f_d) is lost to the surface using the traditional deposition velocity (v_d) approach:

$$M_d = m_p(t)\left\{1 - e^{\left(\frac{-v_d * dt}{0.5\Delta}\right)}\right\}$$

where m_p is the mass associated with a particle, M_d is the deposited mass during dt, the time step of the dispersion model, and Δ is the grid size in the normal direction of the surface (e.g. dz for a horizontal surface).

Deposition velocity. In the model, the deposition velocity in comprised of two parts: a constant non-settling velocity and a settling velocity (w_s) based on particle size. The non-settling velocity is based on NARAC's material database while the settling velocity is calculated from the particle size using the following formula described by Hinds (1982):

$$w_s = \frac{1}{18}\frac{d_p^2 \rho_p g}{\mu_{air}} C_c$$

where ρ_p is the particle density, g is gravitational acceleration, μ_{air} is the absolute viscosity of air, and C_c is the Cunningham's correction factor (Cunningham, 1910). The correction factor is approximated by:

$$C_c = 1 + \frac{2\lambda}{d_p}\left(1.257 + 0.4e^{-\frac{1.1 d_p}{2\lambda}}\right)$$

where λ is the mean free path of air.

However, for vertical surfaces, the deposition velocity includes only the non-settling term as the gravitational settling term won't be applicable for a vertical surface.

Further development of Aeolus particle deposition will be explored for larger Reynolds number, based on the existing LODI implementation and the literature (Hinds 1982).

4.2 Radioactive Decay Chain Model

The time evolution of nuclide concentrations undergoing serial or linear decay chain is governed by a set of first-order differential equations, called Bateman equations. The decay chain model recently implemented in Aeolus is linked to NARAC's database of more than 200 radionuclides.

The Bateman equations (Bateman 1910) for radioactive decay and production describing the number of atoms, N_i, for each nuclide i in an n-nuclide chain are as follows:

$$\frac{dN_1}{dt} = -\lambda_1 N_1$$

$$\frac{dN_i}{dt} = \lambda_{i-1} N_{i-1} - \lambda_i N_i \qquad (i = 2, n)$$

where λ_i is the decay constant of i^{th} nuclide.

Assuming zero atoms of all daughters at time zero: $N_1(0) \neq 0$ and $Ni(0)=0$ when $i > 1$, then the number of atoms of n^{th} nuclide after time t is given by Bateman, as follows:

$$N_n(t) = \frac{N_1(0)}{\lambda_n} \sum_{i=1}^{n} \lambda_1 \alpha_i e^{-\lambda_i t}$$

where

$$\alpha_i = \prod_{\substack{j=1 \\ j \neq i}}^{n} \frac{\lambda_j}{(\lambda_j - \lambda_i)}$$

Example. Technetium-99m is a metastable nuclear isomer, as indicated by the "m" after its mass number 99. A metastable isomer is a decay product whose nucleus remains in an excited state that lasts much longer than is typical. Tc-99m decays mainly by gamma emission, slightly less than 88% of the time.

$$(^{99m}\mathrm{Tc} \rightarrow {}^{99}\mathrm{Tc} + \gamma)$$

Tc-99m's half-life of 6.0058 hours is considerably longer (by 14 orders of magnitude, at least) than most nuclear isomers, though not unique. After gamma emission or internal conversion, the resulting ground-state Technetium-99 then decays with a half-life of 211,000 years to stable Ruthenium-99. This process emits soft beta radiation without a gamma.

$$^{99m}_{43}Tc \xrightarrow[6\ hr\ half\ life]{} {}^{99}_{43}Tc \xrightarrow[211{,}000\ yr\ half\ life]{} {}^{99}_{44}Ru(stable)$$

An Aeolus calculation of the decay of 1 mol of Tc-99m using the Bateman equations is shown in Figure 11.

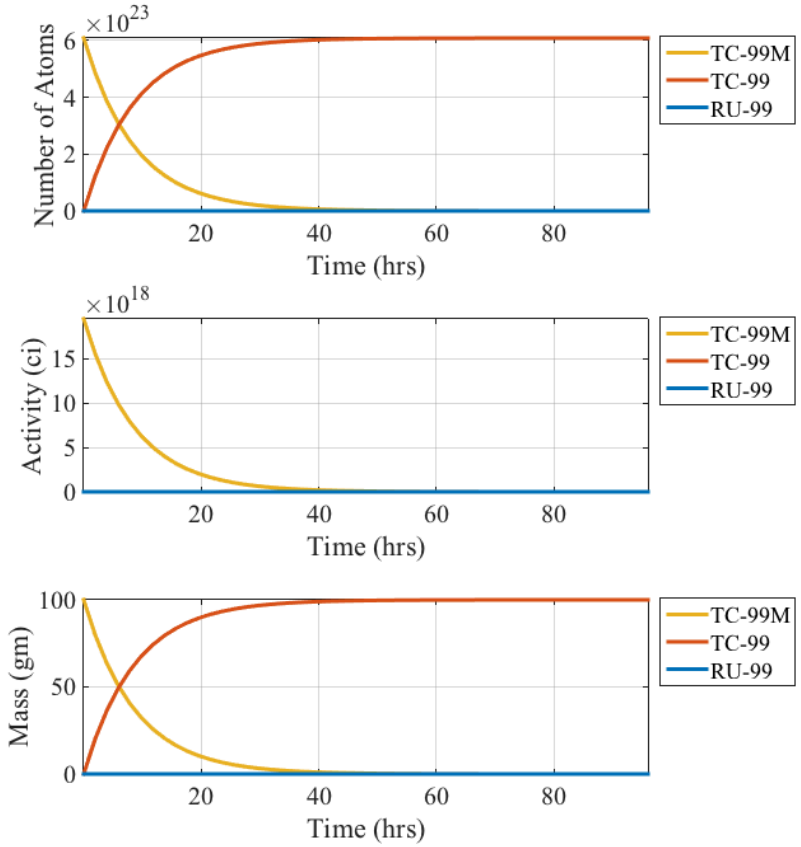

Figure 11: Model produced decay chain of Tc-99m. (at *t*=0, Tc-99m=100 gm).

4.3 RDD Source Term Model

For the specific release of radiological material via an explosive detonation, four distinct phases must be considered when modeling the fate of the airborne particles. The first consideration is to accurately represent the post-detonation size range of the particles which are initially distributed in the fireball. Second, the entrainment of ambient air into the hot gas cloud and the rise rate of the buoyant gases will influence the motion of the particulate material. The third phase is to accurately simulate the subsequent detrainment of these particles from the rising hot gases (how the particles separate from the rising cloud and move outside its influence). Finally, after detrainment, the particle motion is dictated by the ambient (non-thermally-buoyant) atmospheric conditions (mean wind and turbulence). Leveraging tools in the NARAC modeling suite, Aeolus has been updated to include an explosive RDD source term.

NARAC uses the PUFF explosive cloud rise code developed by Sandia National Laboratories (Boughton and DeLaurentis 1987) to predict the time-dependent vertical rise rate and size of a spherical cloud representing the buoyant gas cloud resulting from an explosive detonation. PUFF is an integral model that integrates the three-dimensional conservation of mass, momentum and energy equations over the cloud cross-section. It returns macroscopic cloud properties that form a top-hat profile, where properties have a single averaged value within the cloud and are at ambient conditions outside the boundaries of the cloud. The PUFF-calculated cloud vertical velocity is used in a subsequent Aeolus simulation to lift particles entrained within the cloud.

Previous studies (Woodward 1959, Foster 1982) simulated detrainment based on a comparison between the particle's gravitational settling velocity (w_s) and the buoyant cloud's vertical rise velocity (w_c). In this an approach, larger particles, with correspondingly larger settling velocities, detrain more rapidly than smaller particles. A simple threshold relationship that detrains particles based on the relative magnitudes of their vertical rise and settling velocities was implemented in Aeolus; particles are detrained when $w_c \leq \alpha\ w_s$, where α has been adjusted based on experimental data sets (Neuscamman et al, 2015).

As the cloud of hot explosive products rises from the ground, it expands and cools as ambient air is entrained into the cloud. While they are still inside the cloud, the simulated particles receive both an additional vertical velocity as the cloud rises due to buoyancy and an additional radial velocity to adjust particle position due to cloud expansion.

4.3.1 Validation of Aeolus Using RDD Field Experiments

Green Field I. The Green Field I (GFI) project consisted of a series of explosive detonations to primarily study the resulting time-dependent particulate material cloud rise associated with the thermal buoyancy of the gases produced by detonations of 0.25 to 50(+) kg of high-explosive (Sharon et al, 2012). Aeolus simulations were performed to model the field experiments. Figure 12, below, shows an example of the time evolution of the particles affected by the cloud-rise as predicted by the model.

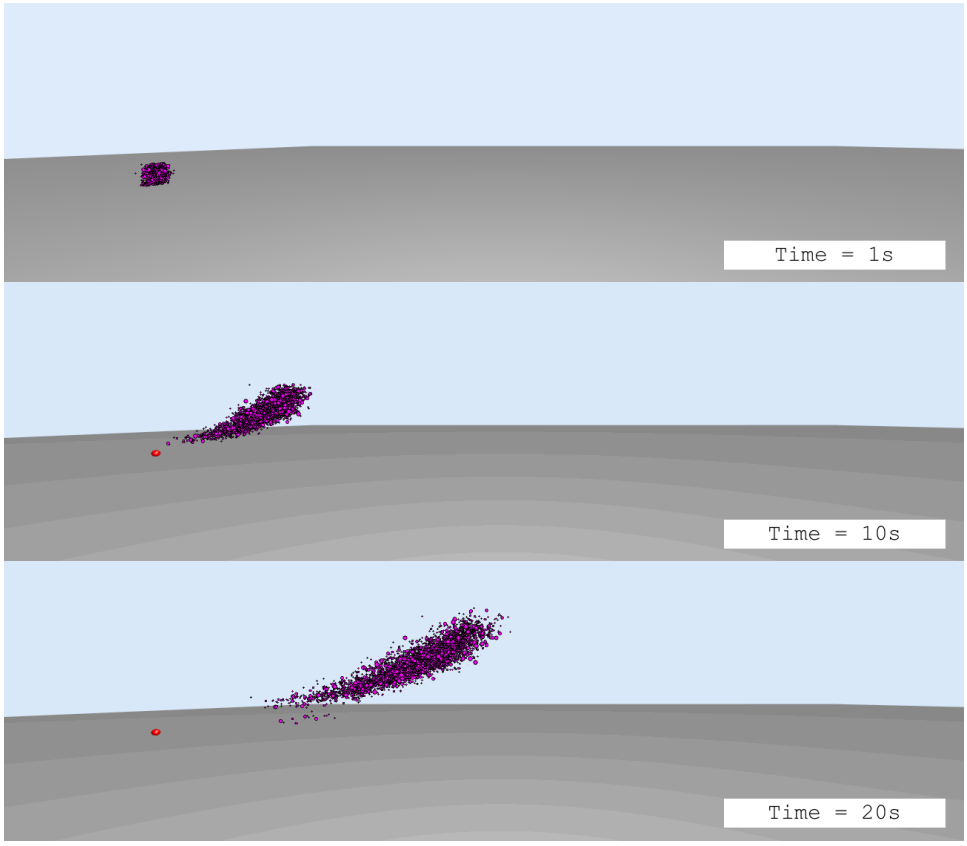

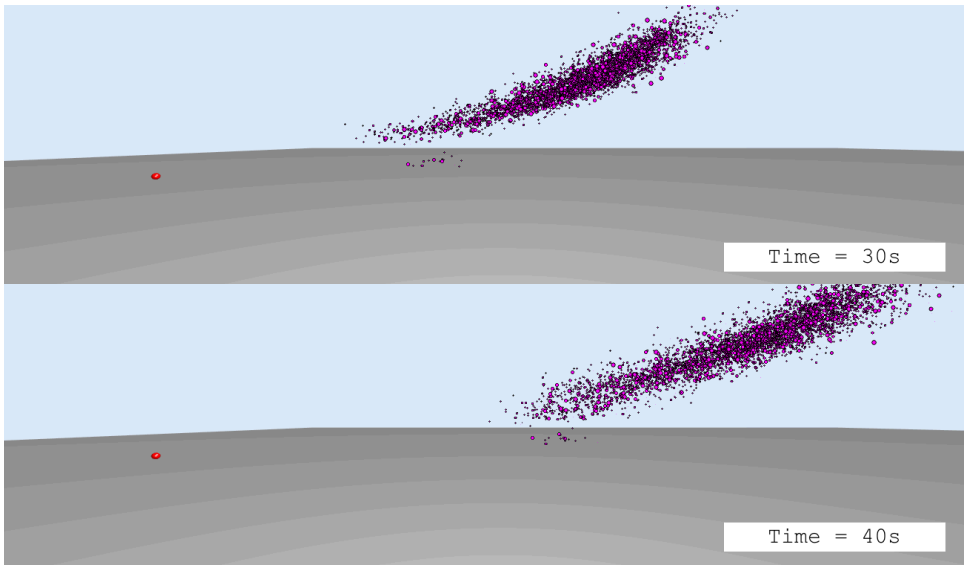

Figure 12: Example of particles carried by an Aeolus cloud rise prediction as a function of time for a 2.0 kg HE detonation, shown in 3D perspective view. Red dot shows the detonation location at ground level.

The following figures show the measured values of cloud top determined from the experiment for three different charge sizes: 0.25 kg (Figure 13), 2.0 kg (Figure 14), and 20.0 kg (Figure 15). The Aeolus cloud rise model predicts the measured data well for a range of charge size.

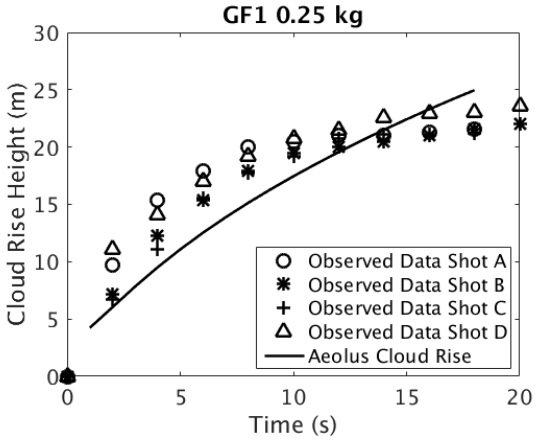

Figure 13: Aeolus predictions of cloud rise from a 0.25 kg HE detonation (line) compared to measured values (symbols).

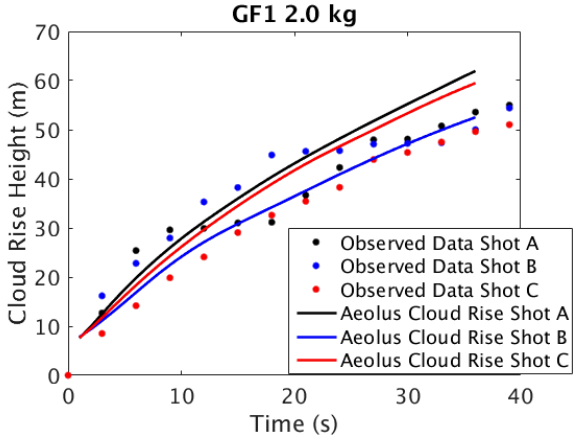

Figure 14: Aeolus predictions of cloud rise from a 2.0 kg HE detonation (line) compared to measured values (symbols). Different colors represent data sets taken under different meteorological conditions.

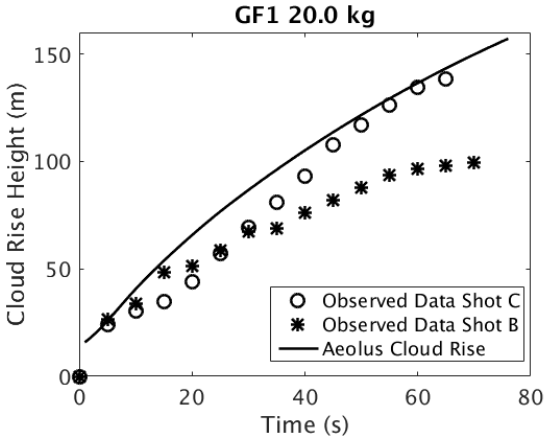

Figure 15: Aeolus predictions of cloud rise from a 20.0 kg HE detonation (line) compared to measured values (symbols).

2012 Canadian RDD Field Trials. A series of three explosive RDD experiments was conducted in 2012 by Defense Research and Development Canada (DRDC) and collaborating organizations from Canada, the US and the UK (Green et al 2016). In order to characterize the dispersion and deposition of radioactive material from an RDD, a source of La-140 (which has a half-life of 1.6781 days) was dispersed by detonation of 0.2 kg of high explosive in each of the three tests.

Measurements of the subsequent dispersion and deposition were made using multiple experimental techniques. Witness plates allowed for localized beta measurements using AB100 beta detectors at 350 locations. The beta measurements of deposition on the witness plate array represent well characterized data with good spatial resolution. The detector and measurement grid used in the experiment are shown in Figure 15. These data were used in a previous model improvement effort, to update the detrainment algorithm in NARAC's LODI dispersion code (Neuscamman et al, 2015).

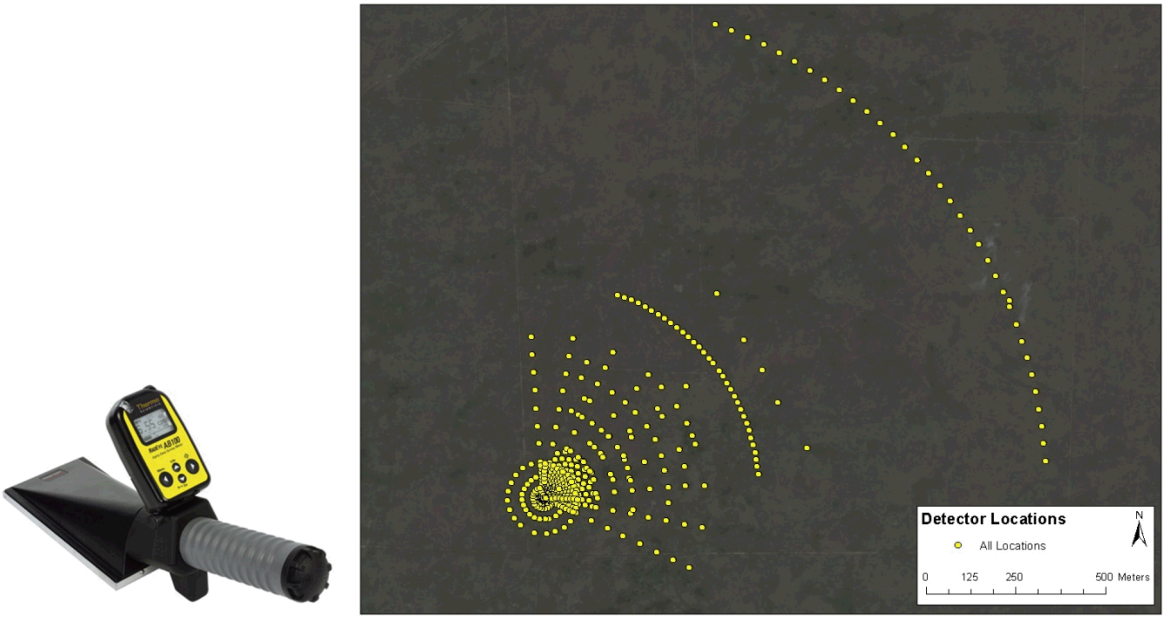

Figure 15: AB100 beta detectors used in the Canadian Full-Scale RDD trials (left) and the 350 measurement locations (right).

Modeled results are compared to measured deposition data collected June 6, 2012 ("shot 1"). The Aeolus model prediction of deposition for shot 1 is shown in Figure 16. There is some discrepancy in the wind direction; the measured centerline is a few degrees off the Aeolus prediction near the detonation location, while further out the discrepancy is a few degrees in the other direction. This may be the result of wind measurements taken during the field trials not being able to measure small changes in winds at the test location during the detonation and plume passage. The downwind extent of the predicted deposition contour levels generally agrees with the measured values. The crosswind spreading of the plume is also well predicted by the model.

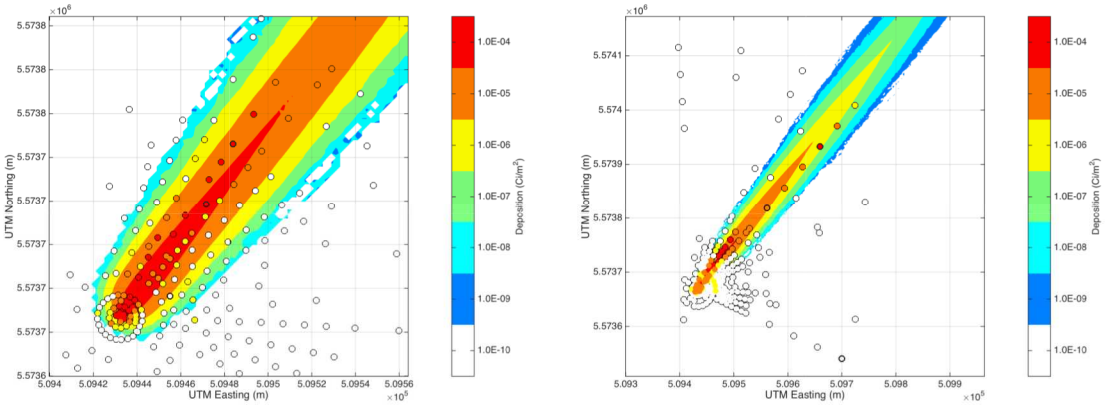

Figure 16: Aeolus deposition results compared to the Canadian Full-Scale RDD field trials shot 1 (June 6, 2012). Right: extent of plume compared to measurement grid; Left: zoomed image showing near release comparison. The colored circles represent the measured data; white circles are near or below the device measurement detectability threshold (0.3μCi/m^2). The contours show predicted deposition concentration (Ci/m2) on a log scale. Each step change in color along the gradient represents an order of magnitude change in concentration.

5. Conclusions

Aeolus is a fast-running CFD urban dispersion model that has been validated using several experimental data sets. Using the Aeolus RANS wind field model and Lagrangian dispersion model, complex dispersal experiments can be completed with simulation run times small enough for use in emergency response, to provide consequence management information. Two recent improvements to Aeolus further enhance the model's applicability for use in these situations: the addition of a radioactive decay chain model based on the Bateman equations, and the implementation of an explosive RDD buoyant source based on NARAC's PUFF/LODI approach to modeling RDD release.

Comparing Aeolus predictions to field experiments, the model generally shows good agreement with the measured data. This report details model validation to the Joint Urban field experiments conducted in 2003 for both continuous and instantaneous tracer gas releases. Aeolus results compare well with measured data both qualitatively and quantitatively. Aeolus simulation of an explosive release is compared to data from the Israeli Green Field and Canadian Full-Scale RDD trials. The agreement between model predictions and measured results is generally good.

Expanding the capabilities of a fast-running urban dispersion model and validating its simulation results against field data greatly advances NARAC's ability to make predictions of the fate of material released in an urban environment. The improved and validated Aeolus model represents a significant capability for NARAC, and improved support to the IMAAC.

6. Future Aeolus Development: FY-18 Efforts

Upcoming work, during the final year of the project, will operationalize the model for use by NARAC analyst to develop and distribute urban modeling products for a RDD release through IMAAC process. The model will utilize input from NARAC databases (e.g., meteorological, terrain and building, radiological materials, decay constants, and dose conversion factor databases) and will be provided as a stand-alone tool for use by NARAC scientific analysts. NARAC analysts will participate in the testing of this tool, and staff training will be provided as part of the model implementation process. The model will be in a form to support future integration into a fully-automated capability, including the generation of more detailed consequence reports and standard briefing products, development of higher-resolution sheltering/shielding calculations, coupling to NARAC's operational product distribution system, coupling to NARAC's existing regional-scale dispersion model, and integration in the next-generation, modernized NARAC operational system framework. The final project report will provide detailed documentation of the new urban modeling capability, including a summary of the validation of the modeling capability against available radiological measurements.

References

Baldwin, B.S. and H. Lomax, 1978: Thin layer approximation and algebraic model for separated turbulent flows, AIAA Paper 78-257.

Bashforth, F., J.C. Adams, 1883: An Attempt to test the Theories of Capillary Action by comparing the theoretical and measured forms of drops of fluid. With an explanation of the method of integration employed in constructing the tables which give the theoretical forms of such drops, Cambridge University Press, Cambridge.

Bateman, H., 1910: Solution of a System of Differential Equations Occurring in the Theory of Radio-active Transformations, Proc. Cambridge Phil. Soc. IS, 423

Boughton B. A., and J. M. Delaurentis, 1987: An Integral Model of Plume Rise from High Explosive Detonations, 1987 ASME/AIChE National Heat Transfer Conference, August 9-12, 1987 Pittsburgh, PA.

Brandt, A. and Livne, O.E., 2011:"Multigrid Techniques: 1984 Guide with Applications to Fluid Dynamics", Revised Edition. Society for Industrial and Applied Mathematics.

Chen, Q., & Xu, W. ,1998: A zero-equation turbulence model for indoor airflow simulation. Energy and buildings, 28(2), 137-144.

Chorin, A.J., 1967: A numerical method for solving incompressible viscous flow problems. Journal of Computational Physics, 2, 12–26.

Clawson, K.L., R.G. Carter, D.J. Lacroix, C.A. Biltoft, N.F. Hukari, R.C. Johnson and J.D. Rich, 2005: Joint Urban 2003 (JU03) SF6 atmospheric tracer field tests. NOAA Technical Memorandum OARARL-254, Air Resources Lab.

Cunningham, E., 1910: "On the velocity of steady fall of spherical particles through fluid medium", Proceedings of the Royal Society A, 83(561), 94-96

Durbin, P. A., 1983: Stochastic differential equations and turbulent dispersion.

Flaherty, J., K.J. Allwine and E. Allwine, 2007: Vertical tracer concentration profiles measured during the Joint Urban 2003 dispersion study. J. of Appl. Met. and Climat. 46(12), 2019–2037.

Foster P. M., 1982: Particle Fallout During Plume Rise, Atmospheric Environment, Vol. 16, No. 12, pp. 2777-2784.

Foster, K. T., G. Sugiyama, J. S. Nasstrom, J. M. Leone Jr., S. T. Chan, B. M. Bowen, 2000: The use of an operational model evaluation system for model intercomparison, Int. J. Environment and Pollution, Vol. 14, pp. 77-88

Gowardhan, A. A., Pardyjak, E. R., Senocak, I., & Brown, M. J., 2011: A CFD-based wind solver for an urban fast response transport and dispersion model. Environmental fluid mechanics, 11(5), 439-464.

Green A. R., L. Erhardt, L. Lebel, M. J. M. Duke, T. Jones, D. White, and D. Quayle, 2016: Overview of the full-scale radiological dispersal device field trials. Health Phys 110(5):403-417

Hanna, S. and Chang, J., 2012: Acceptance criteria for urban dispersion model evaluation. Meteorology and Atmospheric Physics, 116(3-4), pp.133-146.

Hinds, W.C., 1982: "Aerosol Technology", John Wiley and Sons, New York, 424 pp.

Leonard, B. P., 1979: A stable and accurate convective modelling procedure based on quadratic upstream interpolation. Comp. Meth. Appl. Mech. & Eng. 19, p59-98

Lucas, D.D., Gowardhan, A., Cameron-Smith, P. and Baskett, R.L., 2016: "Impact of meteorological inflow uncertainty on tracer transport and source estimation in urban atmospheres", Atmospheric Environment, 143, pp.120-132.

Nelson, M. A., Pardyjak, E. R., Klewicki, J. C., Pol, S. U., & Brown, M. J., 2007: Properties of the wind field within the Oklahoma City Park Avenue street canyon. Part I: Mean flow and turbulence statistics. Journal of Applied Meteorology and Climatology, 46(12), 2038-2054.

Neuscamman S., K. Lennox, K. Yu, K. Foster, and J. Weil, 2015: Improvements to Modeling the Transport and Deposition of Explosive RDD Particulate Material Final Report, LLNL-TR-677619. September 1, 2015.

Prandtl L., 1926: Application of the "Magnus effect" to the wind propulsion of ships. NACA TM 387

Sharon A., I. Halevy, D. Sattinger, I. Yaar, 2012: Cloud rise model for radiological dispersal device events. Atmospheric Environment. 54:603-610; 2012.

Smagorinsky, J., 1963: "General circulation experiments with the primitive equations: I. The basic experiment". Monthly weather review, 91(3), pp.99-164.

Smith, A.M.O. and T. Cebeci, 1967: Numerical solution of the turbulent boundary layer equations. Douglas aircraft division report DAC 33735.

Woodward B., 1959: Motion in and Around Isolated Thermals, Quarterly Journal of the Royal Meteorological Society, Vol. 85, No. 364, pp 144-151.

Warner S, Platt N, Heagy JF, Jordan JE, Bieberbach G, 2006: Comparisons of transport and dispersion model predictions of the mock urban setting test field experiment. J Appl Meteorol 45:1414–1428